

Article

Electrochemical Open-Circuit Voltage and Pressure-Concentration-Temperature Isotherm Comparison for Metal Hydride Alloys

Negar Mosavati ¹, Kwo-Hsiung Young ^{1,2,*}, Tiejun Meng ² and K. Y. Simon Ng ¹

¹ Department of Chemical Engineering and Materials Science, Wayne State University, Detroit, MI 48202, USA; n.mosavati@gmail.com (N.M.); sng@wayne.edu (K.Y.S.N.)

² BASF/Battery Materials-Ovonic, 2983 Waterview Drive, Rochester Hills, MI 48309, USA; tiejun.meng@partners.bASF.com

* Correspondence: kwo.young@basf.com; Tel.: +1-248-293-7000; Fax: +1-248-299-4228

Academic Editor: Andreas Jossen

Received: 27 January 2016; Accepted: 15 March 2016; Published: 23 March 2016

Abstract: In this study we compared the electrochemical pressure-concentration-temperature (EPCT) method with the gaseous phase pressure-concentration-temperature (PCT) method and demonstrated the differences between the two. Experimentally, this was done by electrochemically charging/discharging the electrodes of four different metal hydride (MH) alloys. The results indicate that in the PCT curve is flatter with a smaller hysteresis and a higher storage capacity compared to the EPCT curve. Moreover, while the PCT curves (up to around one third of the hydrogen storage capacity) reside in between the charge and discharge EPCT curves, the rest of the PCT curves are below the EPCT curves. Finally, we demonstrated a new calibration method based on the inflection points observed in the EPCT isotherms of a physical mixture of more than one alloy. This turning point can be used to find a preset calibration point to determine the state-of-charge.

Keywords: metal hydride (MH); electrochemistry; pressure composition isotherm; electrochemical pressure-concentration-temperature (EPCT); state of charge (SOC) estimation

1. Introduction

Nickel/metal hydride (Ni/MH) batteries are an important energy storage medium for portable electronic devices, electric vehicles, and alternative energy. The active material used in the negative electrode (anode) of these batteries is a special kind of metal called hydrogen storage alloy (or metal hydride (MH) alloy) that is capable of storing hydrogen at ambient temperatures [1]. MH alloy can absorb hydrogen in two different environments: through an electrochemical charging process in wet chemistry or gaseous absorption in a dry container (Figure 1). While the former process requires splitting water molecules into protons and hydroxide ions, the latter depends on the splitting of hydrogen molecules into hydrogen atoms. Other differences between the electrochemical charging and gaseous phase hydrogen storage can be found in Table 1. Since the electrochemical environment is more complicated for hydrogen absorption compared to the gaseous phase, the pressure-concentration-temperature (PCT) measurement is commonly used to study the thermodynamics of gaseous phase hydrogen absorption of an MH alloy [1]. The information obtained from PCT, including hydrogen storage capacity, metal-hydrogen bond strength (from the equilibrium pressure), hysteresis, and heat of hydride formation, are all essential for the design of MH alloys used for gaseous hydrogen storage and electrochemical applications. In wet chemistry, the hydrogen storage performance may be heavily influenced by the surface oxide [2], surface catalyst phase [3], proximity effect among phases [4], and activated grain boundary [5], which are difficult to isolate. Therefore, it is

interesting and important to compare the electrochemical and gaseous phase hydrogen storages side by side through comparing the stabilized open-circuit voltage (V_{oc}) *versus* state of charge (SOC) curves in the electrochemical PCT (EPCT) and gaseous phase PCT curves.

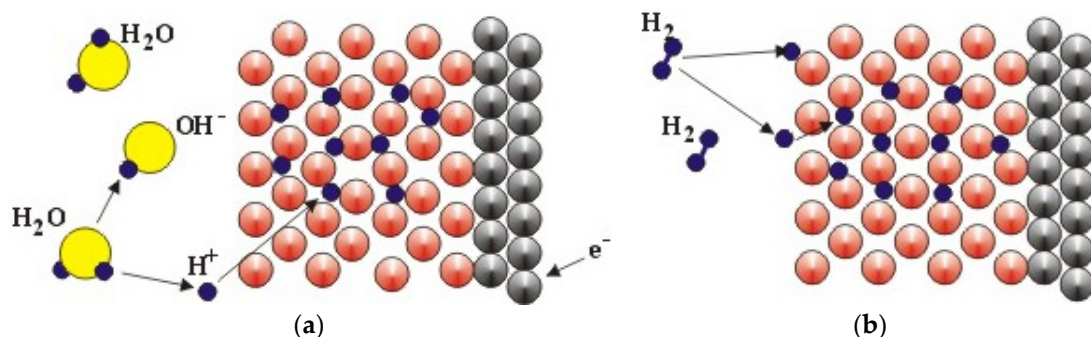


Figure 1. Schematic of hydrogen absorption through (a) an electrochemical reaction and (b) a gaseous phase chemical reaction.

Table 1. The main differences between electrochemical charging and gaseous phase hydrogen storage.

Difference in	Electrochemical Charging	Gaseous Phase Hydrogen Storage
Source of H	Splitting H_2O molecule at the electrode/electrolyte interface	H_2 dissociation at the surface
Environment	Alkaline oxidizing environment (KOH electrolyte)	H_2 gas, very susceptible to oxygen poisoning
Kinetics	Hydrogen storage/release at room temperature	Hydrogen storage/release at temperature range of 20–130 °C
Thermodynamics	ΔH from $-30 \text{ kJ}\cdot\text{mol}\cdot H_2^{-1}$ to $-35 \text{ kJ}\cdot\text{mol}\cdot H_2^{-1}$	ΔH from $-20 \text{ kJ}\cdot\text{mol}\cdot H_2^{-1}$ to $-55 \text{ kJ}\cdot\text{mol}\cdot H_2^{-1}$
Thermal conductivity	Not crucial	Very important
Electrical conductivity	Very important	Not crucial
Chemical reaction	$M + H_2O + e^- \rightleftharpoons MH + OH^-$	$H_2(g) \rightleftharpoons 2H$
Surface requirement	A thin and porous oxide allowing electrolyte penetration	Free from oxide and other contaminations
Common catalyst	Metallic Ni embedded in surface oxide [6]	Noble metals like Pd and Pt [7]

The EPCT method is not a new idea and had been applied in a number of MH alloy studies, including studies on AB₅ [8–11], AB₂-based multiphase alloys [12–14], Ce-Mn-Al-Ni [15], Ce-Mg-Ni-Ti-F [16], carbon nanofiber [17], and Mg₂Ni [18]. In EPCT, the stabilized V_{oc} is converted to equilibrium pressure via the Nernst Equation (1) [19]:

$$E_{MH,eq} (vs. Hg/HgO) = -0.934 - 0.029 \log P(H_2) \quad (1)$$

where $E_{MH,eq}$ is the equilibrium potential of hydrogen storage electrode *versus* the Hg/HgO reference electrode and $P(H_2)$ is the equilibrium hydrogen gas pressure, and the electrochemical capacity is converted to hydrogen storage capacity by using the conversion of $268 \text{ mAh}\cdot\text{g}^{-1} = 1 \text{ wt\%}$. It should be noted that for the Ni/MH half-cell configuration used in this study, a partially pre-charged positive electrode was used and has a constant potential of 0.36 V *versus* Hg/HgO [20], and therefore $E_{MH,eq}$ (*vs.* Hg/HgO) $\approx V_{oc} - 0.36$ (V). Ideally, the stabilized V_{oc} obtained experimentally is close to the battery equilibrium potential.

The advantages of EPCT include simplicity, ease of operation, and ability to cover a wider voltage (pressure) range since a decade of pressure change is equivalent to a voltage difference of 29 mV at

room temperature. It is also closer to the real life environment that batteries experience. Although many studies using EPCT to characterize MH alloys have been reported, a direct comparison between EPCT and the gaseous phase PCT had never been made and is the focus of this paper.

2. Experimental Section

Induction melting with an MgAl_2O_4 crucible, an alumina tundish, and a pancake-shaped steel mold in a 2-kg furnace under argon atmosphere were performed to prepare the ingot samples. AB_5 MH alloys were annealed at 960°C for 8 h under vacuum. Gaseous phase hydrogen storage was measured using a Suzuki-Shokan multi-channel PCT system (Suzuki Shokan, Tokyo, Japan). Each ingot piece (about 2 g) was first activated by a 2 h thermal cycle between room temperature and 300°C under 2.5 MPa H_2 pressure followed by PCT measurements at 30, 60, and 90°C . To fabricate the electrodes for electrochemical tests, the ingot was hydrided and pulverized to -200 mesh powder and pressed onto an expanded Ni substrate without any binder. For EPCT analysis, a flooded half-cell configuration was used with the MH alloy as negative electrode, partially pre-charged and oversized $\text{Ni}_{0.9}\text{Co}_{0.1}(\text{OH})_2$ as counter electrode, and 30 wt% KOH as electrolyte. Before the EPCT measurements, the electrode samples in half-cells were activated with 10 charge/discharge cycles at $25 \text{ mA} \cdot \text{g}^{-1}$ and room temperature using a CTE MCL2 Mini cell test system (Chen Tech Electric MFG. Co., Ltd., New Taipei, Taiwan). Each half-cell was then cycled with several charge/discharge steps, each is 15 min long, at a current density of $25 \text{ mA} \cdot \text{g}^{-1}$ and with a 30 min rest between each step. The electrochemical V_{oc} was recorded at the end of the 30 min rest after each charge/discharge step.

3. Results and Discussion

EPCTs of four MH alloys are included in this study, and their compositions and some gaseous phase properties are listed in Table 2. Fe1 is a C14-predominated AB_2 MH alloy developed in a previous Fe-addition study [21]. B37 and B65 are misch metal-based AB_5 MH alloys with very different equilibrium plateau pressures (Figure 2). The last alloy, YC#1, is a transition metal-based AB_5 MH alloy developed in a study of a series of $\text{ZrV}_x\text{Ni}_{4.5-x}$ alloys showing a large discrepancy between gaseous phase and electrochemical hydrogen storage capacities [22]. EPCTs of these alloys will be reported in the following sections.

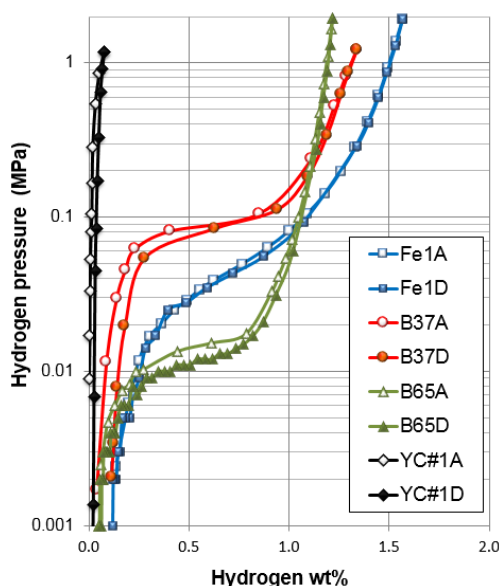


Figure 2. PCT isotherms of alloys in this study. Fe1 is a Fe-containing AB_2 metal hydride (MH) alloy. B37 and B65 are misch metal-based AB_5 MH alloys. YC#1 is a ZrNi_5 -based MH alloy. Open and filled symbols stand for absorption and desorption isotherms, respectively.

Table 2. Design composition and hydrogen storage properties (at 30 °C) of the alloys in this study.
PCT: pressure-concentration-temperature.

Alloy	Family	Composition (in at%)	Maximum H-storage Capacity	Desorption Plateau Pressure	PCT Hysteresis
Fe1	AB ₂	Ti ₁₂ Zr _{21.5} V ₁₀ Cr _{7.5} Mn _{8.1} Fe _{1.0} Co _{7.0} Ni _{32.2} Sn _{0.3} Al _{0.4}	1.51 wt%	0.046 MPa	0.05
B37	AB ₅	La _{9.6} Ce _{4.0} Pr _{0.5} Nd _{1.3} Ni _{65.8} Co _{4.6} Mn _{4.2} Al _{5.5} Cu _{4.6}	1.34 wt%	0.088 MPa	0.06
B65	AB ₅	La _{10.5} Ce _{4.3} Pr _{0.5} Nd _{1.4} Ni _{62.3} Co _{5.0} Mn _{4.6} Al _{6.0} Cu _{3.2} Zr _{0.2} Mo _{2.0}	1.21 wt%	0.012 MPa	0.28
YC#1	AB ₅	Zr _{18.2} Ni _{81.8}	0.075 wt%	>1 MPa	1.76

3.1. Electrochemical Pressure-Concentration-Temperature of AB₂ Metal Hydride Alloy

Room EPCT without re-calibration from Fe1 is shown in Figure 3a. Due to hydrogen gas evolution in the open-cell configuration, the starting point of the charge curve does not match the ending point of the discharge curve. After performing a self-discharge calibration, we found the capacity loss due to hydrogen gas evolution is linear with regard to SOC (from 0% to 100%), and the capacity loss for Fe1 is about $(0.3 + 1.2 \times \text{SOC}) \text{ mAh} \cdot \text{g}^{-1} \cdot \text{h}^{-1}$. The higher SOC of the electrode promotes increased hydrogen gas escaping from the electrode surface. After this calibration, the EPCT charge and discharge curves for Fe1 form a closed loop (Figure 3b). Compared to the PCT isotherm in the same graph, four observations can be made:

- (1) The EPCT curve is much more slanted than the PCT curve.
- (2) The hysteresis of EPCT is much larger than that of PCT, which has been demonstrated previously by Wójcik and his coworkers [13].
- (3) The maximum capacity measured from EPCT is smaller than that from PCT, which has also been previously shown by Wójcik and his coworkers [13].
- (4) The PCT isotherm is closer to the EPCT charge curve when the hydrogen storage content is small, but as the hydrogen storage content increases, it then moves to the center between the EPCT charge and discharge curves and finally flattens out.

The higher hysteresis (asymmetry) in EPCT compared to that in PCT (Observation 2) is related to the difference in equilibrium state. In the gaseous phase equilibrium state, hydrogen concentration in the alloy bulk is uniform. However, in the electrochemical open-circuit condition, distribution of protons is uneven if there is a voltage across the electrode. Therefore, V_{oc} during the charge state (high concentration of OH⁻ in the pores of surface oxide layer) and discharge state (lower concentration of OH⁻ in the pores of surface oxide layer due to water recombination) are different. In the open-circuit condition, the levels of hydrogen storage content in various parts of the electrode are different depending on the distance to surface, which results in a composite of hydrogen storage phases (components) with different metal-hydrogen bond strengths. This phenomenon increases the degree of disorder and lowers the critical temperature to where the PCT plateau disappears [23,24] and thus makes the EPCT curve more slanted (Observation 1).

As for the lower electrochemical capacity seen in EPCT compared to that in PCT (Observation 3), it is a very common observation in MH alloys [25,26]. Surface oxidation during the activation step in the electrochemical environment is one of the causes. In addition, some inter-grain phases acting as catalysts in the gaseous phase [27] can be etched away in the electrochemical environment [5]. In the open-cell configuration, the electrode cannot be fully charged due to hydrogen evolution, which can also contribute to the lower capacity measured by EPCT.

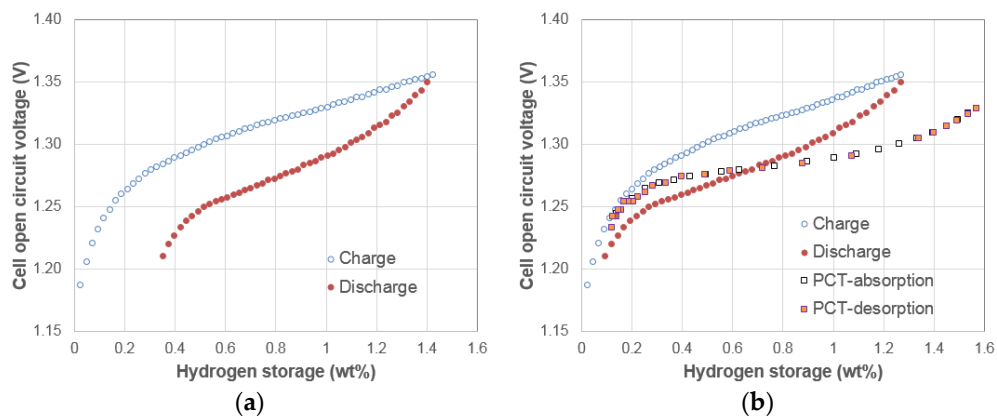


Figure 3. Room temperature electrochemical pressure-concentration-temperature (EPCTs) for Fe1: (a) before and (b) after taking self-discharge into consideration.

Observation 4 implies that the assumption of two-electron transfer with H_2 in Equation (1) is only valid at lower SOCs. As the hydrogen storage content increases, the electrochemical reaction becomes closer to the interaction with single H atoms, which will raise the voltage as dictated by the Nernst equation with single electron transfer Equation (2):

$$E_{MH,eq} \text{ (vs. Hg/HgO)} = -0.934 - 0.059\log P(H_2) \quad (2)$$

3.2. Electrochemical Pressure-Concentration-Temperatures of Two AB_5 Metal Hydride Alloys

Room EPCTs of two AB_5 alloys with a large difference in plateau pressure, B37 and B65, were measured, and the charge and discharge curves after self-discharge calibration are shown in Figure 4. All four observations made in the previous section of the AB_2 MH alloy are also present for the AB_5 MH alloys. Therefore, these observations are likely to be universal for most MH alloys. Comparing these two EPCTs, the alloy with a lower PCT plateau pressure (B65) has a higher electrochemical capacity than the alloy with a higher PCT plateau pressure (B37), and hence the proposed cause for lower EPCT capacity discussed in the last section (incomplete charging due to hydrogen gas evolution) is validated.

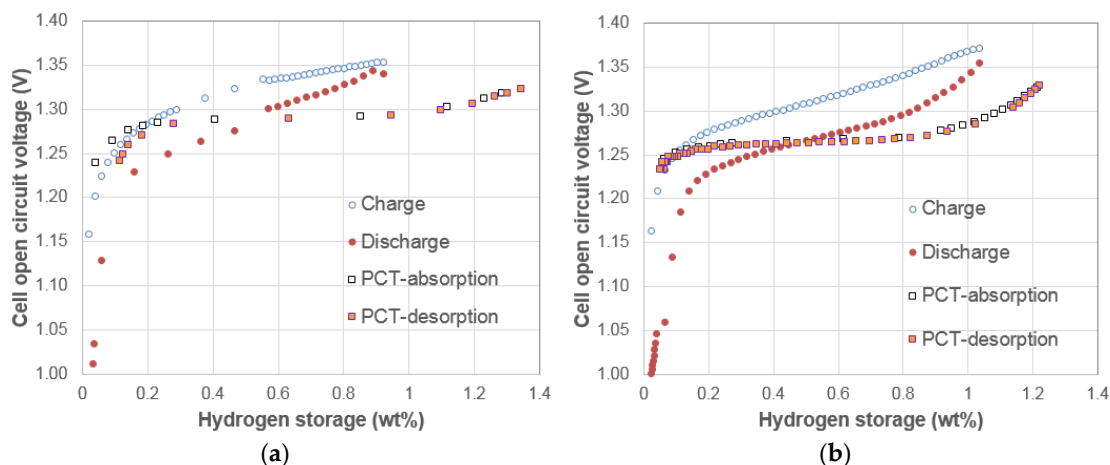


Figure 4. Room temperature EPCTs for (a) B37 and (b) B65 after taking self-discharge into consideration.

3.3. Electrochemical Pressure-Concentration-Temperatures of Mixtures of Two AB_5 Metal Hydride Alloys

PCTs of materials with two phases (components) were classified into three categories: funneling mode, synergistic mode, and independent mode [4,28]. If two MH alloys were physically mixed

together without any alloying, the resulting PCT isotherm will be a composite showing two individual plateaus (Figure 7c in [4]). It is interesting to see whether the discontinuity in the PCT isotherm of two-part alloy is present in the corresponding EPCT isotherm. If the discontinuity exists in the EPCT isotherm, it will contribute tremendously to SOC determination, which relies heavily on V_{oc} and impedance (Z) in today's battery management systems [29–35]. However, V_{oc} and Z depend not only on SOC but also on the state-of-health and environmental temperature, making a precise calculation of SOC impossible.

Room temperature EPCTs of B37/B65 mixtures (10:90, 30:70 and 50:50 by weight) are shown in Figure 5a–c, respectively. Discontinuities in slope can easily be found in both the charge and discharge curves in Figure 5a,b. In the case of the 50:50 mixture, the derivative of V_{oc} versus hydrogen storage content is plotted in Figure 5d to show the locations of the inflection points (when the derivative reaches the local maximum). The existence of these inflection points confirms the possibility of using V_{oc} to find a preset calibration point for SOC determination.

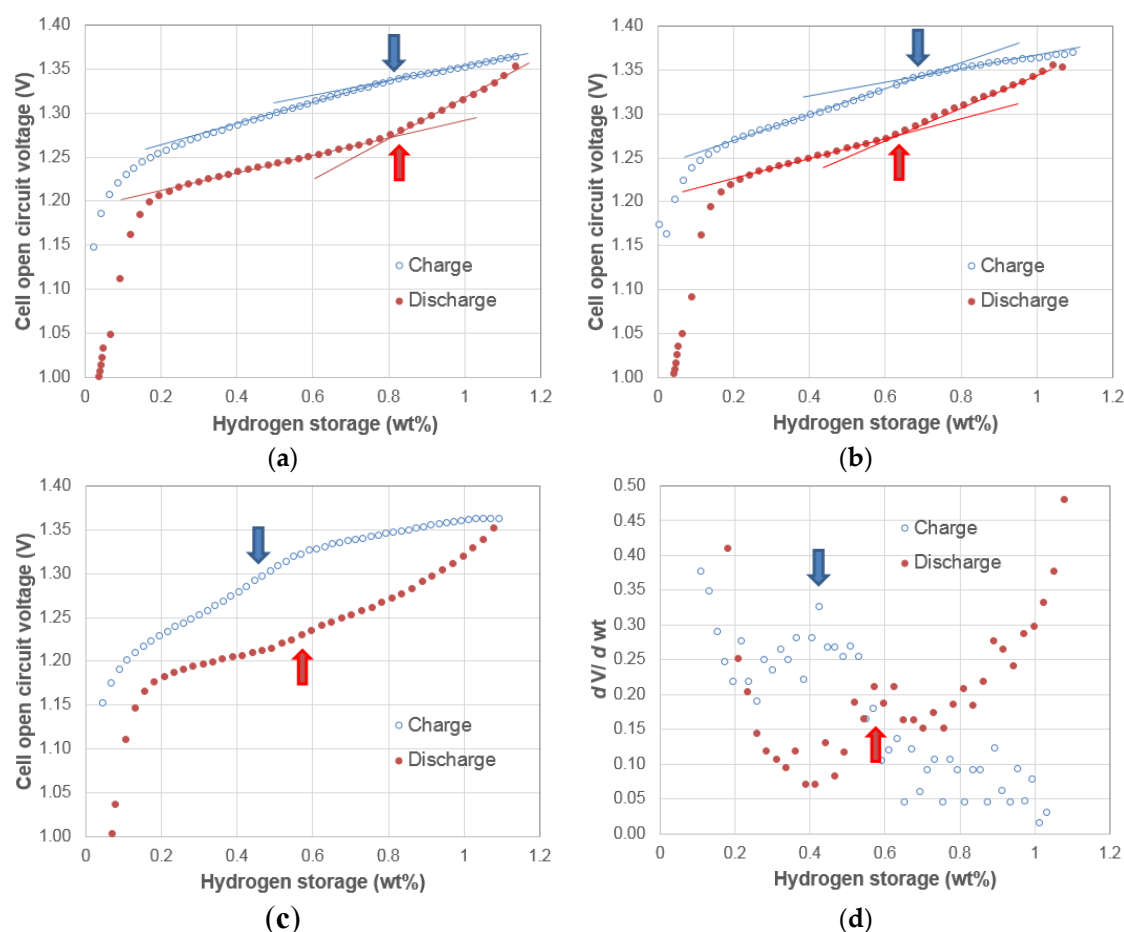


Figure 5. Room temperature EPCTs for (a) 10% B37 + 90% B65; (b) 30% B37 + 70% B65; (c) 50% B37 + 50% B65 mixtures and (d) derivative of Figure 5c. Arrows indicate positions of inflection points.

In order to investigate whether the existence of inflection points is sensitive to the environment temperature, EPCT of the B37/B65 50:50 mixture was measured at 10 °C. The resulting charge and discharge curves are shown in Figure 6a and clearly show the inflection points at approximately 50% SOC. Moreover, Figure 6b shows the derivative of V_{oc} versus hydrogen storage content, which can be used to better locate the inflection points.

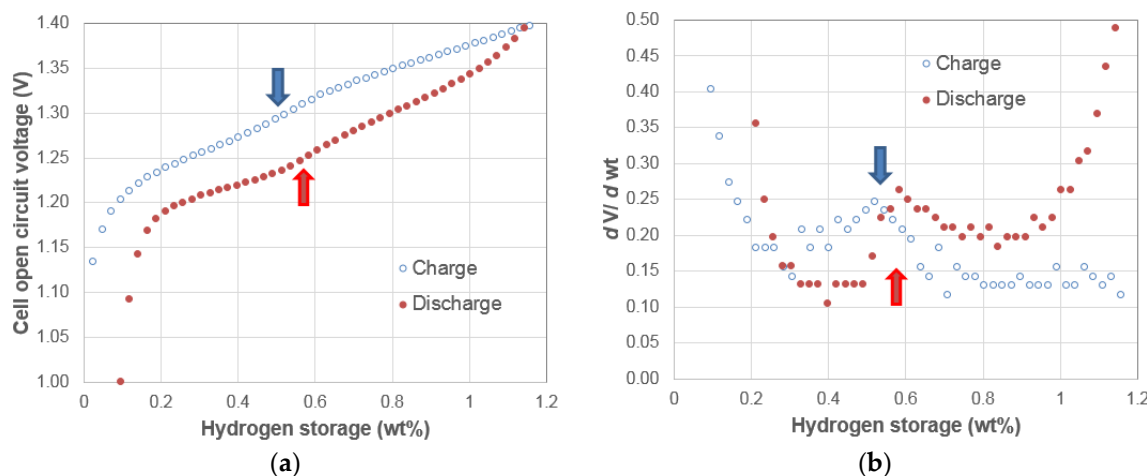


Figure 6. 10 °C: (a) EPCT and (b) derivative for 50% B37 + 50% B65 mixture. Arrows indicate positions of inflection points.

3.4. Electrochemical Pressure-Concentration-Temperature of $\text{ZrNi}_{4.5}$ Metal Hydride Alloy

In studies of multiphase Zr-Ni-V MH alloys, we found that the electrochemical capacities of these alloys were unusually high compared to the gaseous phase hydrogen storage capacities [22,36], which had been attributed to the decrease in PCT plateau pressure through synergetic effects in the electrochemical environment [22,36]. We now compare EPCT and PCT of one of those alloys, YC#1, in Figure 7. It is obvious that the charge and discharge curves are below the PCT curves with the assumption that the same correlation from AB_2 (Figure 3b) and AB_5 (Figure 4a,b) can be applied in YC#1. Therefore, we confirm that our previous statement: lowering the equilibrium pressure in the electrochemical environment is the main cause of increased capacity.

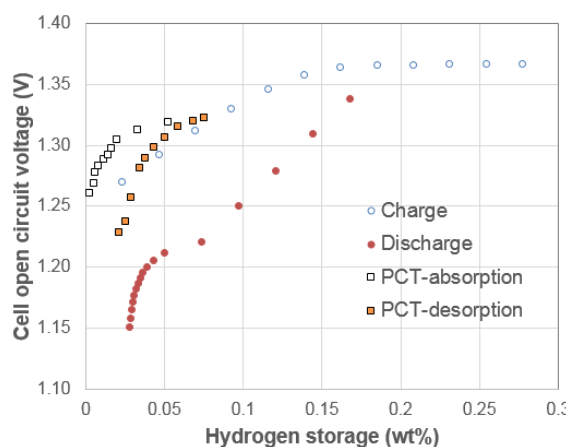


Figure 7. Room temperature EPCT for YC #1.

3.5. Discussion

The difference between PCT and EPCT results can be explained by the different natures of hydrogen storage processes in a single component hydrogen storage alloy (or metal) system. For hydrogen absorption in the gaseous phase, hydrogen gas molecules adsorb and split into two hydrogen atoms at the clean surface of metal (free from oxide), and then hydrogen atoms move into the bulk of alloy by diffusion. The protons occupy the interstitial sites among the host atoms while the accompanied electrons join the conduction band of host metal and increase the Fermi level of conduction electrons. In the electrochemical environment, the applied voltage forces electrons to

flow into the negative electrode and also splits the water molecules at the electrode surface. While the protons enter the bulk of alloy driven by the electric field from the potential difference and are neutralized by the electrons from the current collector, the hydroxide ions are released into the electrolyte. Moreover, the equilibrium pressure in the gaseous phase is only dependent on the concentration of hydrogen in the metal, but what affects V_{oc} in the electrochemical environment is far more complicated and involves the dipole from the electrolyte-solid interface, chemical products from the activation process, and potential between the bulk and altered surfaces with different chemical compositions from the bulk. The discharge processes for the gaseous phase and electrochemistry are also different. In the gaseous phase, the movement of protons is intrigued by diffusion, and equilibrium is reached when the same amount of hydrogen is leaving and entering the metal. However, it is more complicated in the electrochemical environment. During discharge, electrons move away from the hydrided alloy into the current collector, forcing the protons to move in the opposite direction and reach the electrode surface. Unless the surface recombination of either proton-hydroxide or proton-oxygen is very slow (not likely) and a large amount of protons accumulation presents at the electrode-electrolyte interface, the protons should continue to flow towards the interface in order to reach charge neutrality until a depletion of protons.

Hystereses found in EPCT of the AB_2 and AB_5 MH alloys are much larger than the corresponding hysteresis in PCT. While the hysteresis observed in PCT can be simplified as the energy barrier of elastic deformation at the α - β interface during hydrogenation [37], many other factors can influence the hysteresis in EPCT, such as the potential between the activated surface region and bulk, potential across the surface oxide region and oxide in the activated grain boundaries [38], remaining charge trapped within the defects and grain boundaries, residual protons trapped in the grain boundaries, and distribution of hydroxide ions in the surface pores and grain boundaries that are connected to the electrolyte by narrow channels.

Hydrogen storage in a multiphase alloy system is by far more complicated due to the presence of synergetic effects. Synergetic effects in multiphase MH alloys refer to the beneficial effects provided by the presence of micro-segregated secondary phases occurred in the melted alloys [39], which were reviewed, explained, and compared between gaseous phase and electrochemistry in one of our recent publications [40] and can be summarized as follows: the contact potential at the boundary between two neighboring phases with different work functions resulted from the increase in the Fermi level of the side with a lower Fermi level by the addition of electrons into the conduction band from the substituted hydrogen. This remaining hydrogen at the very end of dehydrogenation will act as the nucleation center for the β -phase (MH). It will also facilitate the hydrogenation process with a much reduced PCT hysteresis as seen from Figure 2—two single component AB_5 MH alloys (large hysteresis) and one multiphase AB_2 MH alloy (small hysteresis).

The above description, in general, works for both gaseous phase and electrochemistry. However, the synergetic effects in electrochemistry are more profound than those in the gaseous phase. With additional potential difference present across the alloy, the grain boundary acts as a liaison between two phases (changing from charged side to the uncharged side, resulting in two partially charged sides). The sharp transition in gaseous phase equilibrium pressure will not be seen in the electrochemical environment. In a separate article, a group of MH alloys composed of BCC and non-BCC (TiNi, C14, and Ti_2Ni) phases show two distinctive pressure plateaus in PCT but no noticeable jump or change in the slope of electrochemical charge/discharge curves even though x-ray diffraction analysis indicates the transformation from the completion of hydrogenation of the non-BCC phases (lower equilibrium pressure) to the start of hydrogenation of the BCC phase (higher equilibrium pressure) [40]. In the current study, the equivalent equilibrium pressure in the electrochemical environment of the phase with a higher plateau pressure ($ZrNi_5$) is lowered by the synergetic effects from the phase with a lower plateau pressure (Zr_2Ni_7).

According to our experience, the comparison between PCT and EPCT measurements is summarized in Table 3. Advantages of EPCT over PCT are its lower cost, ease of operation,

ability to cover a wider voltage (pressure) range, and similarity to the real battery environment. The disadvantages of EPCT are that it is difficult to perform phase identification (catalyst *versus* storage) and separate the contributions from the surface and alloy bulk; it is also insensitive to several important MH alloy characteristics (metal-hydrogen bond strength, homogeneity, degree of disorder in both alloy and hydride, *etc.*).

Table 3. The comparison between PCT and EPCT techniques.

Aspect	PCT	EPCT
Main application	Gaseous phase hydrogen storage	Electrochemistry
Set-up	Valve, pressure gauge, vacuum pump, and heater	Basic electrochemical station
Equipment cost	~\$20,000 USD per channel	~\$1000 USD per channel
Sample size	0.5 g to 2 g	100 mg to 100 g
Sample shape	Ingots	–200 mesh powder
Pre-condition	Fresh cleavage or acid etched	Hot alkaline bath or electrochemical cycling
Main safety concern	Hydrogen gas safety; powder after PCT measurement can be highly pyrophoric	Cycled electrode after drying can be pyrophoric
Temperature range	–20 °C to 200 °C	–40 °C to 50 °C
Equivalent pressure range	0.0001 MPa to 10 MPa	Wider than 1 Pa to 1000 MPa
Synergetic effects in multiphase alloy	Determined mainly by the difference in metal-hydrogen bond strength	Determined by the difference in work function
Properties obtained	Storage capacity, metal-hydrogen bond strength, thermodynamic, hydride/dehydride hysteresis, and interaction among phases	Storage capacity up to 1 atm, contribution from the activated surface
Not suitable for	Alloys with very high or very low plateau pressure, alloys with poor surface catalytic abilities, alloys in the fine particle form	Alloys with low corrosion resistance in alkaline solution, alloys with high plateau pressure (>1 atm), alloys with very large hardness or ductility

4. Conclusions

Electrochemical PCT isotherms were obtained for several MH alloys. The results after self-discharge calibration show differences between gaseous phase PCT and EPCT. EPCT isotherm measurements of the AB₂ and AB₅ MH alloys prove that the PCT curves are much flatter than the curves for EPCT. PCT also has a smaller hysteresis and higher capacity. Moreover, when the hydrogen storage content is small, the PCT isotherm is closer to the EPCT charge curve. However, as the hydrogen storage content increases, the PCT isotherm then moves to the center between the EPCT charge and discharge curves and finally flattens out. In addition, previous and current studies on the multiphase Zr-Ni-V MH alloy (YC#1) demonstrate that the plateau pressure reduction in the electrochemical environment due to synergetic effects is the main cause of the increase in electrochemical discharge capacity compared to the gaseous phase measurements. Furthermore, it was found that the inflection points in the EPCT isotherm of a physical mixture of more than one alloy can be used to find a preset calibration point for measurement of SOC.

Acknowledgments: The authors would like to thank the following for their assistance: from BASF-Ovonic: Lixin Wang, Taihei Ouchi, Baoquan Huang, Jean Nei, Diana F. Wong, David Pawlik, Allen Chan, Ryan J. Blankenship, and Su Cronogue.

Author Contributions: Kwo-Hsiung Young and Tiejun Meng conceived and designed the experiments; Negar Mosavati performed the experiments; Negar Mosavati and Kwo-Hsiung Young analyzed the data; Kwo-Hsiung Young and K. Y. Simon Ng wrote the paper.

Conflicts of Interest: The authors declare no conflict of interest.

References

- Young, K. Metal Hydrides. In *Reference Module in Chemistry, Molecular Sciences and Chemical Engineering*; Reedijk, J., Ed.; Elsevier: Waltham, MA, USA, 2012. [[CrossRef](#)]
- Young, K.; Chao, B.; Liu, Y.; Nei, J. Microstructures of the oxides on the activated AB₂ and AB₅ metal hydride alloys surface. *J. Alloy. Compd.* **2014**, *606*, 97–104. [[CrossRef](#)]
- Young, K.; Wong, D.F.; Nei, J.; Reichman, B. Electrochemical properties of hypo-stoichiometric Y-doped AB₂ metal hydride alloys at ultra-low temperature. *J. Alloy. Compd.* **2015**, *643*, 17–27. [[CrossRef](#)]
- Wong, D.F.; Young, K.; Nei, J.; Wang, L.; Ng, K.Y.S. Effects of Nd-addition on the structural, hydrogen storage, and electrochemical properties of C14 metal hydride alloys. *J. Alloy. Compd.* **2015**, *647*, 507–518. [[CrossRef](#)]
- Young, K.; Chang, S.; Chao, B.; Nei, J. Microstructures of the activated Si-containing AB₂ metal hydride alloy surface by transmission electron microscope. *Batteries* **2016**, *2*. [[CrossRef](#)]
- Young, K.; Huang, B.; Regmi, R.K.; Lawes, G.; Liu, Y. Comparisons of metallic clusters imbedded in the surface of AB₂, AB₅, and A₂B₇ alloys. *J. Alloy. Compd.* **2010**, *506*, 831–840. [[CrossRef](#)]
- Song, J.; Meng, B.; Tan, X.; Liu, S. Surface-modified proton conducting perovskite hollow fibre membranes by Pd-coating for enhanced hydrogen permeation. *Int. J. Hydrol. Energy* **2015**, *40*, 6118–6127. [[CrossRef](#)]
- Bliznakov, S.; Lefterova, E.; Bozukov, L.; Popov, A.; Andreev, P. Techniques for Characterization of Hydrogen Absorption/Desorption in Metal Hydride Alloys. In Proceedings of the International Workshop Advanced Techniques for Energy Source Investigation and Testing, Sofia, Bulgaria, 4–9 September 2004; pp. 19-1–19-6.
- Raju, M.; Ananth, M.V.; Vijayaraghaven, L. Influence of temperature on the electrochemical characteristics of MmNi_{3.03}Si_{0.85}Co_{0.60}Mn_{0.31}Al_{0.08} hydrogen storage alloys. *J. Power Sources* **2008**, *180*, 830–835. [[CrossRef](#)]
- Feng, F.; Ping, X.; Zhou, Z.; Geng, M.; Han, J.; Northwood, D.O. The relationship between equilibrium potential during discharge and hydrogen concentration in a metal hydride electrode. *Int. J. Hydrol. Energy* **1998**, *23*, 599–602. [[CrossRef](#)]
- Bliznakov, S.; Lefterova, E.; Dimitrov, N. Electrochemical PCT isotherm study of hydrogen absorption/desorption in AB₅ type intermetallic compounds. *Int. J. Hydrol. Energy* **2008**, *33*, 5789–5794. [[CrossRef](#)]
- Kopczyk, M.; Wójcik, G.; Mlynarek, G.; Sierczyńska, A.; Bełtowska-Brzezinska, M. Electrochemical absorption-desorption of hydrogen on multicomponent Zr-Ti-V-Ni-Cr-Fe alloys in alkaline solution. *J. Appl. Electrochem.* **1996**, *26*, 639–645. [[CrossRef](#)]
- Wójcik, G.; Kopczyk, M.; Mlynarek, G.; Majchrzycka, W.; Bełtowska-Brzezinska, M. Electrochemical behavior of multicomponent Zr-Ti-V-Ni-Cr-Fe alloys in alkaline solution. *J. Power Sources* **1996**, *58*, 73–78. [[CrossRef](#)]
- Zhu, Y.F.; Pan, H.G.; Gao, M.X.; Ma, J.X.; Li, S.Q.; Wang, Q.D. The effect of Zr substitution for Ti on the microstructures and electrochemical properties of electrode alloys Ti_{1-x}Zr_xV_{1.6}Mn_{0.32}Cr_{0.48}Ni_{0.6}. *Int. J. Hydrol. Energy* **2015**, *40*, 6118–6127. [[CrossRef](#)]
- Hou, C.; Zhao, M.; Li, J.; Huang, L.; Wang, Y.; Yue, M. Enthalpy change (ΔH°) and entropy (ΔS°) measurement of CeMn_{1-x}Al_{1-x}Ni_{2x} ($x = 0.00, 0.25, 0.50$ and 0.75) hydrides by electrochemical P-C-T curve. *Int. J. Hydrol. Energy* **2008**, *33*, 3762–3766. [[CrossRef](#)]
- Hu, F.; Zhang, Y.; Zhang, Y.; Hou, Z.; Dong, Z.; Deng, L. Microstructure and electrochemical hydrogen storage characteristics of CeMg₁₂ + 100wt%Ni + Ywt%TiF₃ ($Y = 0, 3, 5$) alloys prepared by ball milling (in Chinese). *J. Inorg. Mater.* **2013**, *28*, 217–223. [[CrossRef](#)]
- Kudo, H.; Unno, K.; Kamegawa, A.; Takamura, H.; Okada, M. Synthesis and protium absorption properties of vapor growth carbon nano-fibers grown by Fe-based catalyst. *Mater. Trans.* **2002**, *42*, 1127–1132. [[CrossRef](#)]
- Yang, H.; Zhang, H.; Mo, W.; Zhou, Z. Mg_{1.8}La_{0.2}Ni-xNi nanocomposites for electrochemical hydrogen storage. *J. Phys. Chem. B* **2006**, *110*, 25769–25774. [[CrossRef](#)] [[PubMed](#)]
- Kleperis, J.; Wójcik, G.; Czerwinski, A.; Showronski, J.; Kopczyk, M.; Bełtowska-Brzezinska, M. Electrochemical behavior of metal hydride. *J. Solid State Electrochem.* **2001**, *5*, 229–249. [[CrossRef](#)]
- Watanabe, K.; Koseki, M.; Kumagai, N. Effect of cobalt addition to nickel hydroxide as a positive material for rechargeable alkaline batteries. *J. Power Sources* **1996**, *58*, 23–28. [[CrossRef](#)]

21. Young, K.; Ouchi, T.; Huang, B.; Reichman, B.; Fetcenko, M.A. The structure, hydrogen storage, and electrochemical properties of Fe-doped C14-predominating AB₂ metal hydride alloys. *Int. J. Hydrol. Energy* **2011**, *36*, 12296–12304. [[CrossRef](#)]
22. Young, K.; Young, M.; Chang, S.; Huang, B. Synergetic effects in electrochemical properties of ZrV_xNi_{4.5-x} ($x = 0.0, 0.1, 0.2, 0.3, 0.4$, and 0.5) metal hydride alloys. *J. Alloy. Compd.* **2013**, *560*, 33–41. [[CrossRef](#)]
23. Young, K.; Huang, B.; Ouchi, T. Studies of Co, Al, and Mn substitutions in NdNi₅ metal hydride alloys. *J. Alloy. Compd.* **2012**, *543*, 90–98. [[CrossRef](#)]
24. Sun, D.; Jiang, J.; Lei, Y.; Liu, W.; Wu, J.; Wang, Q. Effects of measurement factor on electrochemical capacity of some hydrogen storage alloys. *Mater. Sci. Eng. B* **1995**, *30*, 19–22. [[CrossRef](#)]
25. Chang, S.; Young, K.; Ouchi, T.; Meng, T.; Nei, J.; Wu, X. Studies on incorporation of Mg in Ti-based AB₂ metal hydride alloys. *Batteries* **2016**, *2*. submitted.
26. Young, K.; Fetcenko, M.A.; Li, F.; Ouchi, T. Structural, thermodynamic, and electrochemical properties of Ti_xZr_{1-x}(VNiCrMnCoAl)₂ C14 Laves phase alloys. *J. Alloy. Compd.* **2008**, *464*, 238–247. [[CrossRef](#)]
27. Iba, H.; Akiba, E. Hydrogen absorption and modulated structure in Ti-V-Mn alloys. *J. Alloy. Compd.* **1997**, *253–254*, 21–24. [[CrossRef](#)]
28. Young, K.; Ouchi, T.; Huang, B.; Reichman, B.; Blankenship, R. Improvement in -40°C electrochemical properties of AB₂ metal hydride alloy by silicon incorporation. *J. Alloy. Compd.* **2013**, *575*, 65–72. [[CrossRef](#)]
29. Bundy, K.; Karlsson, M.; Lindbergh, G.; Landqvist, A. An electrochemical impedance spectroscopy method for prediction of the state of charge of a nickel-metal hydride battery at open circuit and during discharge. *J. Power Sources* **1998**, *72*, 118–125. [[CrossRef](#)]
30. Slepiski, P.; Darowicki, K.; Janicka, E.; Sierczynska, A. Application of electrochemical impedance spectroscopy to monitoring discharging process of nickel/metal hydride battery. *J. Power Sources* **2013**, *241*, 121–126. [[CrossRef](#)]
31. Pop, V.; Bergveld, H.J.; Notten, P.H.L.; Reftien, P.P.L. State-of-the-art of battery state-of-charge determination. *Meas. Sci. Technol.* **2005**, *16*, R93–R110. [[CrossRef](#)]
32. Williams, M.; Mackie, C.; Barbour, P.W. Method and Apparatus for Determining the State of Charge of a Battery. U.S. Patent 4,958,127, 18 September 1990.
33. Galbraith, R.E.; Gisi, J.M.; Norgaard, S.P.; Reetz, D.D.; Ziebarth, D.J. Method and Apparatus for Estimating the Service Life of a Battery. U.S. Patent 6,191,556 B1, 20 February 2001.
34. Lim, J.H.; Ji, S.; Han, S. Method for Measuring SOC of a Battery Management System and the Apparatus Thereof. U.S. Patent 8,548,761, 1 October 2013.
35. Zhang, Y.; Du, X.; Salman, M.A.; Huang, S. Battery SOC Estimation with Automatic Correction. U.S. Patent 9,108,524, 18 August 2015.
36. Young, M.; Chang, S.; Young, K.; Nei, J. Hydrogen storage properties of ZrV_xNi_{3.5-x} ($x = 0.0\text{--}0.9$) metal hydride alloys. *J. Alloy. Compd.* **2013**, *580*, S171–S174. [[CrossRef](#)]
37. Young, K.; Ouchi, T.; Fetcenko, M.A. Pressure-composition-temperature hysteresis in C14 Laves phase alloys: Part 1. Simple ternary alloys. *J. Alloy. Compd.* **2009**, *480*, 428–433. [[CrossRef](#)]
38. Young, K.; Chao, B.; Pawlik, D.; Shen, H.T. Transmission electron microscope studies in the surface oxide on the La-containing AB₂ metal hydride alloy. *J. Alloy. Compd.* **2016**. [[CrossRef](#)]
39. Visintin, A.; Peretti, A.A.; Fruiz, F.; Corso, H.L.; Triaca, W.E. Effect of additional catalytic phases imposed by sintering on the hydrogen absorption behavior of AB₂ type Zr-based alloys. *J. Alloy. Compd.* **2007**, *428*, 244–251. [[CrossRef](#)]
40. Young, K.; Ouchi, T.; Meng, T. Studies in synergetic effects in multi-phase metal hydride alloys. *Batteries* **2016**, *2*. submitted.



© 2016 by the authors; licensee MDPI, Basel, Switzerland. This article is an open access article distributed under the terms and conditions of the Creative Commons by Attribution (CC-BY) license (<http://creativecommons.org/licenses/by/4.0/>).